Inorganic Chemistry
Article

Inorg. Chem. **2009**, *48*, 9409–9418 **9409**
DOI: 10.1021/ic901251w

Syntheses, Structures, and Magnetic Properties of Nickel-Doped Lepidocrocite Titanates

Tao Gao,*,† Poul Norby,‡ Hiroshi Okamoto,† and Helmer Fjellvåg†

†*Centre for Materials Science and Nanotechnology and Department of Chemistry, University of Oslo, P.O. Box 1033, N-0315 Oslo, Norway, and* ‡*Materials Research Division, Risø National Laboratory for Sustainable Energy, Technical University of Denmark, P.O. 49, DK-4000 Roskilde, Denmark*

Received June 30, 2009

Ni-doped titanate $Cs_xTi_{2-x/2}Ni_{x/2}O_4$ and its protonic derivative $H_xTi_{2-x/2}Ni_{x/2}O_4 \cdot xH_2O$ ($x = 0.7$) were synthesized and characterized by means of synchrotron X-ray diffraction, Raman scattering, X-ray photoelectron spectroscopy (XPS), and magnetic measurements. $Cs_xTi_{2-x/2}Ni_{x/2}O_4$ crystallizes in an orthorhombic structure (space group *Immm*), consisting of infinite two-dimensional (2D) host layers of the lepidocrocite (γ-FeOOH) type. The substitution of Ni atoms for Ti in the 2D octahedral layers results in negative charges that are compensated by interlayer Cs^+ ions. Raman scattering and XPS indicate that local structural perturbations are induced upon exchange of interlayer Cs ions with protons H_3O^+. Magnetic measurements reveal typical paramagnetism induced by Ni substitution; the effective paramagnetic moment $\mu_{eff} = 1.57(1)\ \mu_B$ and Curie−Weiss temperature $-2.51(1)$ K are obtained for $H_xTi_{2-x/2}Ni_{x/2}O_4 \cdot xH_2O$. Ni- and Mg-codoped titanates $Cs_xTi_{2-x/2}(Ni_yMg_{1-y})_{x/2}O_4$ ($x = 0.7$, $0 \leq y \leq 1$) were also reported. The crystal structure, interlayer chemistry, and magnetic properties of the titanates depend on the Ni substitution levels, indicating opportunities for tuning of the properties by controlling the nature and level of lattice substitutions.

Introduction

Heterovalent substitution (or doping when considering minute concentrations) is recognized as a strong means of modifying materials' properties. Usually, such substitution/doping modifies the electronic properties and, hence, the transport and magnetic properties. Likewise the chemical properties and stability are likely to be changed. Controlling the type and concentration of the substituents/dopants is therefore a key issue. For example, local magnetic moments can be introduced into diamagnetic semiconductors by doping with 3d transition-metal (TM) atoms such as Fe, Co, Ni, and Mn.[1,2] This process results in diluted magnetic semiconductors that integrate semiconducting and ferromagnetic functionalities and are key components for many spin-based devices.[1−5] The report of room temperature ferromagnetism in Co-doped TiO_2 thin films[3,4] has spurred considerable interest in the search for high-T_c ferromagnetism in wide-band-gap oxides doped with TM atoms.[5] However, in such systems, there is an inherent tendency to phase segregation above the solid solubility limit; therefore, it has become difficult to determine whether the observed ferromagnetism is an intrinsic effect due solely to the magnetic atom substitutions or an extrinsic effect due to the presence of magnetic secondary phases.[6]

In oxides like TiO_2, the very stable structure usually prevents any larger degree of heterovalent substitution/doping.[7] On the other hand, certain titanate oxides of perovskite[8] or lepidocrocite type (i.e., layered titanates with γ-FeOOH-type layered structure)[9] show huge flexibility to accommodate 3d TM atoms by substitution and thereby play important roles in the exploration of new materials with interesting properties. Lepidocrocite titanates are of particular interest

*To whom correspondence should be addressed. E-mail: tao.gao@kjemi.uio.no.

(1) (a) Žutić, I.; Fabian, J.; Das Sarma, S. *Rev. Mod. Phys.* **2004**, *76*, 323–410. (b) Wolf, S. A.; Awschalom, D. D.; Buhrman, R. A.; Daughton, J. M.; von Molnár, S.; Roukes, M. L.; Chthelkanova, A. Y.; Treger, D. M. *Science* **2001**, *294*, 1488–1495.
(2) (a) Felser, C.; Fecher, G. H.; Balke, B. *Angew. Chem., Int. Ed.* **2007**, *46*, 668–699. (b) Furdyna, J. K. *J. Appl. Phys.* **1988**, *64*, R29–R64.
(3) Matsumoto, Y.; Murakami, M.; Shono, T.; Hasegawa, T.; Fukumura, T.; Kawasaki, M.; Ahmet, P.; Chikyow, T.; Koshihara, S.; Koinuma, H. *Science* **2001**, *291*, 854–856.
(4) Chambers, S. A.; Thevuthasan, S.; Farrows, R. F. C.; Marks, R. F.; Thiele, J. U.; Folks, L.; Samant, M. G.; Kellock, A. J.; Ruzycki, N.; Ederer, D. L.; Diebold, U. *Appl. Phys. Lett.* **2001**, *79*, 3467–3469.
(5) (a) Prellier, W.; Fouchet, A.; Mercey, B. *J. Phys.: Condens. Matter* **2003**, *15*, R1583–R1601. (b) Dietl, T. *Semicond. Sci. Technol.* **2002**, *17*, 377–392. (c) Liu, W. K.; Whitaker, K. M.; Kittilstved, K. R.; Gamelin, D. R. *J. Am. Chem. Soc.* **2006**, *128*, 3910–3911.
(6) Ohno, H. *Science* **1998**, *281*, 951–956.
(7) Jarzebski, Z. M. *Oxide Semiconductors*; Pergamon: Oxford, U.K., 1973.
(8) Nakayama, H.; Yoshida, H. K. *Jpn. J. Appl. Phys.* **2001**, *40*, L1355–L1358.
(9) Reid, A. F.; Mumme, W. G.; Wadsley, A. D. *Acta Crystallogr.* **1968**, *B24*, 1228–1233.

Published on Web 09/10/2009

for several reasons. They comprise a large class of isomorphous compounds with composition $A_xTi_{2-y}M_yO_4$, where $x = 0.7$, 0.75, or 0.8 for A = Cs, Rb, or K, respectively, and M represents a vacancy or Li, Mg, Zn, Cu, Co, Ni, Fe^{II}, Fe^{III}, Mn^{III}, Sc, or Al.[9−16] Structurally, lepidocrocite titanates consist of two-dimensional (2D) corrugated layers of edge- and corner-shared octahedra with interlayer alkali ions that compensate for the negative charge of the layers due to substitution of lower-valence metal atoms or vacancies for Ti.[9−17] The interlayer ions are exchangeable with a variety of inorganic or organic cations.[13,14,16−19] Moreover, lepidocrocite titanates can be delaminated into molecular single sheets (i.e., the 2D octahedral host layers) of composition $[Ti_{1-y/2}M_{y/2}O_4]^{-x/2}$ under given conditions.[17,20,21] These nanosheets have unique 2D morphological features and anisotropic properties, representing ideal building blocks for the assembly of artificial nanoarchitectures with intentional and controllable functionalities.[22]

The formulation $A_xTi_{2-y}M_yO_4$ indicates that lepidocrocite titanates are intrinsic heavily doped materials and, e.g., ferromagnetism is expected upon the introduction of certain 3d TM atoms.[15,17] Previously, Reid et al. reported the synthesis and crystal structure of $Rb_xTi_{2-x}Mn_xO_4$ (x = 0.75), $Cs_xTi_{2-x}Mn_xO_4$ ($x = 0.7$), and $Cs_xTi_{2-x}Fe_xO_4$ (x = 0.67).[9] Later, Birchall et al. studied the magnetic properties of $Cs_xTi_{2-x}Fe_xO_4$ and $Cs_xTi_{2-x}Sc_{x-y}Fe_yO_4$ ($x = 0.67$ and y = 0.02, 0.05, 0.10, 0.20, and 0.67).[15] Recently, Osada et al. observed room-temperature ferromagnetism and interesting magnetooptical effects in $Ti_{1-x/4}Co_{x/4}O_2$ nanosheets delaminated from a Co-doped titanate $K_xTi_{2-x/2}Co_{x/2}O_4$ (x = 0.8).[17] For Ni-doped phases, less work has so far been reported. Groult et al. studied crystal structures of K-loaded lepidocrocite titanates and reported a composition of $K_{0.80}Ti_{1.6}Ni_{0.4}O_4$;[12] Nakano et al. reported pressure-induced intercalation of alcohol molecules into $K_{0.80}Ti_{1.6}Ni_{0.4}O_4$.[23] However, no detailed data on physical or chemical properties were presented, except for unit cell dimensions.

The motivation for the current study of Ni-doped lepidocrocite titanates is manifold; first, Ni substitution into the dielectric titanate matrix can readily be achieved, which will provide the synthetic basis for clarifying whether Ni-doped TiO_2 thin films display ferromagnetism or just paramagnetism dependent on synthetic conditions;[24,25] second, Ni doping is reported to enhance the photocatalytic performance in a number of semiconductors.[26,27] It would be highly interesting to achieve a similar enhancement in lepidocrocite titanates that already are well-known for exhibiting photocatalytic reactivities.[28,29] In this work, the Ni-doped lepidocrocite titanate $Cs_xTi_{2-x/2}Ni_{x/2}O_4$ ($x = 0.7$) is synthesized and its corresponding protonic form $H_xTi_{2-x/2}Ni_{x/2}O_4 \cdot xH_2O$ is obtained via acid exchange. The magnetic measurements reveal paramagnetic behavior for both of these Ni-doped titanates. Moreover, a codoping approach that is feasible to vary the Ni concentration at the Ti site is developed by introducing both Ni and Mg in the titanates, i.e., $Cs_xTi_{2-x/2}(Ni_yMg_{1-y})_{x/2}O_4$ ($x = 0.7$ and $0 \le y \le 1$). The resemblance of the oxidation state of Ni and Mg will maintain the described charge compensation scheme and thus prevent any phase separation, offering opportunities to elucidate the likely doping-dependent physiochemical properties.

Experimental Section

Reagents and Materials. Cesium carbonate Cs_2CO_3 (99.9%), anatase TiO_2 (99.9%), nickel oxide NiO (97%), magnesium oxide MgO (99%), and tetrabutylammonium hydroxide (TBAOH hereafter) aqueous solution (40 wt %), all from Sigma-Aldrich Co., were used as received. Double-distilled water was used throughout the study.

Ni-doped lepidocrocite titanate $Cs_xTi_{2-x/2}Ni_{x/2}O_4$ ($x = 0.7$) was prepared via a conventional solid-state reaction.[13] For a typical synthesis, a well-mixed powder of stoichiometric amounts of Cs_2CO_3, NiO, and TiO_2 was heated in an alumina crucible at 800 °C for 30 min for removal of carbonate. The mixture was thereafter ground, pelletized, and subjected to two heating cycles (each 950 °C, 20 h) with intermediate grinding. The obtained product was light-green with micrometer-sized powder particles.

Ni- and Mg-codoped titanates with composition $Cs_xTi_{2-x/2}(Ni_yMg_{1-y})_{x/2}O_4$ ($x = 0.7$ and $0 \le y \le 1$) were prepared in order to modify the Ni substitution level while retaining the charge compensation scheme. Well-mixed powders of Cs_2CO_3, NiO, MgO, and TiO_2 in relevant stoichiometric ratios were treated similarly to the Ni route described above. Also, the end member of the series $Cs_xTi_{2-x/2}Mg_{x/2}O_4$ ($x = 0.7$), synthesized previously,[13b] was presently studied.

Protonic forms of the synthesized materials were obtained by acid leaching. A total of 200 mg of the as-prepared titanate was dispersed in 100 mL of a H_2SO_4 aqueous solution (1 M) and ion-exchanged at room temperature for 3 days. The acid solution was renewed every day. The solid material was finally filtered off

(10) Hervieu, M.; Raveau, B. *Rev. Chim. Minér.* **1981**, *18*, 642–649.
(11) Grey, I. E.; Li, C.; Madsen, I. C.; Watts, J. A. *J. Solid State Chem.* **1987**, *66*, 7–19.
(12) Groult, D.; Mercy, C.; Raveau, B. *J. Solid State Chem.* **1980**, *32*, 289–296.
(13) (a) England, W. A.; Birkett, J. E.; Goodenough, J. B.; Wiseman, P. J. *J. Solid State Chem.* **1983**, *49*, 300–308. (b) Gao, T.; Fjellvåg, H.; Norby, P. *J. Mater. Chem.* **2009**, *19*, 787–794.
(14) Sasaki, T.; Kooli, F.; Iida, M.; Michiue, Y.; Takenouchi, S.; Yajima, Y.; Izumi, F.; Chakoumakos, B. C.; Watanabe, M. *Chem. Mater.* **1998**, *10*, 4123–4128.
(15) Birchall, T.; Greenwood, N. N.; Reid, A. F. *J. Chem. Soc. A* **1969**, *16*, 2382–2398.
(16) Gao, T.; Fjellvåg, H.; Norby, P. *Chem. Mater.* **2009**, *21*, 3503–3513.
(17) (a) Osada, M.; Ebina, Y.; Fukuda, K.; Ono, K.; Takada, K.; Yamaura, K.; Takayama-Muromachi, E.; Sasaki, T. *Phys. Rev. B* **2006**, *73*, 153301 (4 pages). (b) Osada, M.; Ebina, Y.; Takada, K.; Sasaki, T. *Adv. Mater.* **2006**, *18*, 295–299. (c) Osada, M.; Itose, M.; Ebina, Y.; Ono, K.; Ueda, S.; Kobayashi, K.; Sasaki, T. *Appl. Phys. Lett.* **2008**, *92*, 253110 (3 pages).
(18) Suzuki, N.; Hayashi, N.; Honda, C.; Endo, K.; Kanzaki, Y. *Bull. Chem. Soc. Jpn.* **2006**, *79*, 711–716.
(19) Sasaki, T.; Watanabe, M.; Michiue, Y.; Komatsu, Y.; Izumi, F.; Takenouchi, S. *Chem. Mater.* **1995**, *7*, 1001–1007.
(20) (a) Sasaki, T.; Watanabe, M.; Hashizume, H.; Yamada, H.; Nakazawa, H. *J. Am. Chem. Soc.* **1996**, *118*, 8329–8335. (b) Sasaki, T.; Watanabe, M. *J. Am. Chem. Soc.* **1998**, *120*, 4682–4689.
(21) Gao, T.; Fjellvåg, H.; Norby, P. *J. Phys. Chem. B* **2008**, *112*, 9400–9405.
(22) (a) Sasaki, T. *J. Ceram. Soc. Jpn.* **2007**, *115*, 9–16. (b) Osada, M.; Sasaki, T. *J. Mater. Chem.* **2009**, *19*, 2503–2511.
(23) Nakano, S.; Sasaki, T.; Takemura, K.; Watanabe, M. *Chem. Mater.* **1998**, *10*, 2044–2046.
(24) (a) Hong, N. H.; Sakai, J.; Prellier, W.; Hassini, A.; Ruyter, A.; Gervais, F. *Phys. Rev. B* **2004**, *70*, 195204 (5 pages). (b) Hong, N. H.; Sakai, J.; Prellier, W.; Ruyter, A. *J. Phys. D: Appl. Phys.* **2005**, *38*, 816–821.
(25) Minh, N. V.; Khang, N. C.; Yang, I. S. *8th IEEE Conf. Nanotechnol.* **2008**, 797–799.
(26) Kudo, A.; Sekizawa, M. *Chem. Commun.* **2000**, 1371–1372.
(27) Jing, D. W.; Zhang, Y. J.; Guo, L. *J. Chem. Phys. Lett.* **2005**, *415*, 74–78.
(28) (a) Kim, Y. I.; Salim, S.; Huq, M. J.; Mallouk, T. E. *J. Am. Chem. Soc.* **1991**, *113*, 9561–9563. (b) Kim, Y. I.; Atherton, S. J.; Brigham, E. S.; Mallouk, T. E. *J. Phys. Chem.* **1993**, *97*, 11802–11810.
(29) Kudo, A.; Kondo, T. *J. Mater. Chem.* **1997**, *7*, 777–780.

and rinsed with copious water and dried in air at room temperature.

Intercalation of organic amines was performed by dispersing 50 mg of protonic titanate powders into 100 mL of diluted TBAOH solutions (5 wt %). The intercalation reaction was carried out at 60 °C under constant stirring for 1 week. Thereafter, the solid products were filtered, rinsed with copious water, and finally separated from the suspension by centrifugation.

Raman Scattering Spectroscopy. Raman scattering spectra were collected at room temperature in a backscattering configuration; the samples were illuminated by using a 632.8 nm He−Ne laser on an Olympus BX 40 confocal microscope with a 50× objective. The wavenumber stability and accuracy of the apparatus were calibrated by recording the F_{2g} Raman-active mode of silicon at 521 cm^{-1}.

X-ray Photoelectron Spectroscopy (XPS). Around ∼50 mg of the as-prepared materials was pressed into pellets and attached to the XPS sample holder via conductive carbon glue. XPS spectra were collected with a KRATOS Axis Ultra-DLD spectrometer using Al Kα radiation (1486.6 eV). A pass energy of 80 eV with a step size of 1 eV was used for survey scans. For separate photoelectron lines, a pass energy of 20 eV was used with a step size of 0.1 eV. The surfaces of the samples were flooded with low-energy electrons to compensate for electrostatic charging. Energy referencing was based on the C−C component of C 1s at 284.8 eV.[30] All samples were studied at room temperature at a pressure of approximately 10^{-8} Torr. Spectra were analyzed using CasaXPS software (version 1.0.0.1).[31]

Magnetic Measurement. Temperature- and field-dependent magnetic measurements of the as-prepared materials were carried out with a SQUID magnetometer (Quantum Design MPMS). Magnetization measurements were carried out in both field-cooled (FC) and zero-field-cooled (ZFC) modes under a magnetic field of $H = 100$ Oe over a temperature range of $5\ K \leq T \leq 350\ K$. The dependence of magnetization on the magnetic field was collected at 5 K over a field range of $-50\ kOe \leq H \leq 50\ kOe$.

Structural Refinement. Powder synchrotron X-ray diffraction (SXRD) data of the Ni-doped titanate $Cs_xTi_{2-x/2}Ni_{x/2}O_4$ were collected at room temperature using a MAR345 imaging plate system at the Swiss−Norwegian Beamline BM01A, European Synchrotron Radiation Facility (ESRF), Grenoble, France. The sample was loaded into a quartz-glass capillary with an inner diameter of 0.7 mm. SXRD data were measured between $2\theta = 1$ and 40° with a wavelength of 0.694 02 Å and a step interval $2\theta = 0.017\ 83°$. The exposure time used was 20 s. The powder SXRD data were analyzed by the Rietveld method with GSAS[32] using EXPGUI.[33] Starting atomic coordinates for Cs, Ti, Ni, and O were taken from an isomorphous compound $Cs_xTi_{2-x/2}Mg_{x/2}O_4$ ($x = 0.7$) reported previously;[13] the highest symmetry, *Immm*, was assumed in this work. A modified pseudo-Voigt profile function[34] was used. A broad peak at about $2\theta = 11°$ was observed and excluded from the refinements;[13b] the calculated intensity of (110), situated in the excluded region, matches the observed intensity well (see Figure S1 in the Supporting Information).

Characterization. Phase analysis of the obtained materials was based on powder XRD data collected on a Siemens D5000 powder diffractometer (Cu $K\alpha_1$ radiation $\lambda = 0.154\ 06$ nm; pore-size-distribution detector; reflection geometry). The morphology and composition of the samples were analyzed by a scanning electron microscope (FEI Quanta 200F) equipped with an energy-dispersive X-ray spectrometer. Chemical analysis was performed by ALS Scandinavia AB, Oslo, Norway; the samples were dissolved in a mixture of HF and H_2SO_4 aqueous solution and analyzed subsequently by inductively coupled plasma mass spectroscopy (ICP-MS). Thermogravimetric analysis (TGA) was performed on a Perkin-Elmer TGA 7 system in a nitrogen atmosphere at a heating rate of 10 °C min^{-1}.

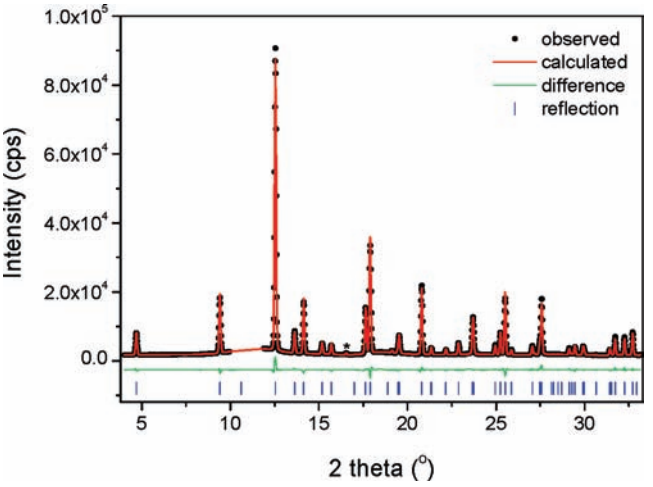

Figure 1. Rietveld fitting of SXRD data of $Cs_xTi_{2-x/2}Ni_{x/2}O_4$ ($x = 0.7$). The region from 9.94° to 11.88° is excluded; see the text and Supporting Information. The asterisk indicates the peak due to trace amounts of NiO impurities. Wavelength: 0.694 02 Å.

Table 1. Results and Relevant Information for the Rietveld Refinement of $Cs_xTi_{2-x/2}Ni_{x/2}O_4$[a]

formula	$Cs_{0.34}(Ti,Mg)O_2$
temperature/K	298
wavelength/Å	0.694 02
pattern range/deg	4−33
space group	*Immm* (No. 71)
a/Å	3.8420(1)
b/Å	16.9051(3)
c/Å	2.9666(1)
V/Å^3	192.682(6)
Z	4
no. of observations	1739
no. of reflns	60
no. of refined param	58
R_{wp}	0.040
R_p	0.030

[a] Calculated standard deviations are in parentheses.

Results and Discussion

Syntheses. The Ni-doped lepidocrocite-type titanate $Cs_xTi_{2-x/2}Ni_{x/2}O_4$ ($x = 0.7$) is a new solid solution phase, although some isomorphous compounds such as $Cs_xTi_{2-x/2}Mg_{x/2}O_4$ ($x = 0.7$)[13] and $K_xTi_{2-x/2}Ni_{x/2}O_4$ ($x = 0.8$)[12,23] have previously been synthesized. Rietveld refinements were performed on the basis of SXRD data for as-prepared $Cs_xTi_{2-x/2}Ni_{x/2}O_4$. The observed, calculated, and difference profiles are illustrated in Figure 1; relevant parameters for the Rietveld refinement are reported in Table 1; atomic coordinates and displacement parameters are given in Table 2 and selected interatomic distances in Table 3.

(30) (a) Briggs, D.; Seah, M. P. *Practical Surface Analysis: Auger and X-Ray photoelectron spectroscopy*, 2nd ed.; Wiley: Chichester, U.K., 1990. (b) Swift, P. *Surf. Interface Anal.* **1982**, *4*, 47–51.
(31) http://www.casaxps.com.
(32) Larson, A. C.; Von Dreele, R. B. *Los Alamos National Laboratory Report LAUR*; Los Alamos National Laboratory, Los Alamos, NM, **1994**; pp 86748
(33) Toby, B. H. *J. Appl. Crystallogr.* **2001**, *34*, 210–213.
(34) (a) Stephens, P. *J. Appl. Crystallogr.* **1999**, *32*, 281–289. (b) Finger, L. W.; Cox, D. E.; Jephcoat, A. P. *J. Appl. Crystallogr.* **1994**, *27*, 892–900.

Table 2. Refined Atomic Coordinates and Equivalent Isotropic Displacement Parameters (Å^2) for $Cs_xTi_{2-x/2}Ni_{x/2}O_4$[a]

atom	position	population	x	y	z	U_{iso}
Cs	4i	0.34	0	0	0.1588(6)	0.0515[c]
M[b]	4h	1	0	0.3100(1)	0.5	0.0117(5)
O1	4g	1	0	0.2204(2)	0	0.0261(9)
O2	4g	1	0	0.3764(2)	0	0.0261(9)

[a] Calculated standard deviations are in parentheses. [b] Virtual species of $0.825Ti^{4+} + 0.175Ni^{2+}$; see the text. [c] $U_{11} = 0.0161(9)$, $U_{22} = 0.028(1)$, $U_{33} = 0.110(3)$, and $U_{12} = U_{13} = U_{23} = 0$.

Table 3. Selected Interatomic Distances (Å) in $Cs_xTi_{2-x/2}Ni_{x/2}O_4$[a]

atoms	distance (Å)	atoms	distance (Å)
M[b]−O1	2.119(2) × 2	Cs−O2	3.013(2) × 4
M−O1	1.988(1) × 2	Cs−O2	3.446(2) × 4
M−O2	1.861(2) × 2	Cs−O1	3.756(3) × 2

[a] Calculated standard deviations are in parentheses. [b] Virtual species of $0.825Ti^{4+} + 0.175Ni^{2+}$.

The refinement of the body-centered orthorhombic structure (space group *Immm*) yielded satisfactory fits and convergence with residual factors $R_{wp} = 0.040$ and $R_p = 0.030$. The refined unit cell dimensions are $a = 3.8420(1)$ Å, $b = 16.9051(3)$ Å, and $c = 2.9666(1)$ Å. This implies an interlayer distance $b/2 \approx 8.45$ Å, similar to that of isomorphous $Cs_xTi_{2-x/2}Mg_{x/2}O_4$ (8.50 Å).[13] All atoms were refined using isotropic displacement parameters except for Cs, where a considerable improvement in the refinement was obtained by introducing anisotropic displacement parameters.[13b] Moreover, a splitting of Cs into the 4i position, $(0, 0, z)$ and $(0, 0, -z)$, is necessary to attain a good fit (Table 2). Analogous splitting of interlayer Cs ions was discussed previously for isomorphous compounds such as $Cs_xTi_{2-x/2}Mg_{x/4}O_4$ ($x = 0.7$)[13b] and $K_xTi_{2-x/3}Li_{x/3}O_4$ ($x = 0.8$).[14] The site occupancy of Ti and Ni atoms was fixed during the refinement (Table 2), following the procedures used for isomorphous compounds such as $K_xTi_{2-x/3}Li_{x/3}O_4$ ($x = 0.8$).[14] Allowing the Ti/Ni ratio to refine results in a stable refinement with a slightly improved goodness of fit, however, the obtained populations, 0.56 and 0.44 for Ti and Ni, respectively, do not give a satisfactory charge balance and do not agree with the original stoichiometry and chemical analysis data. Because the improvement in the fit by releasing the populations is not very large, the resulting cation distribution is probably not reliable. The Ti/Ni ratio is therefore fixed (Table 2).

The refinement confirms that Ni atoms occupy randomly octahedral sites in the 2D corrugated host layers and Cs ions take interlayer positions; substituting Ni^{2+} for Ti^{4+} in the framework results in a negative charge that is balanced by the interlayer Cs^+ ions.[13] This structure type has been described in detail by Reid et al.,[9] and only some features will be elaborated on here. Figure 2a shows the crystal structure for $Cs_xTi_{2-x/2}Ni_{x/2}O_4$ ($x = 0.7$), consisting of 2D infinite layers and interlayer Cs^+ ions. The principle layers are compact and consist of two atomic planes of Ti and four atomic planes of O along the layer normal; the Ti atomic plane is sandwiched in between the O1 (i.e., four-coordinated O atom) and O2 (i.e., two-coordinated O atom) atomic planes, forming a

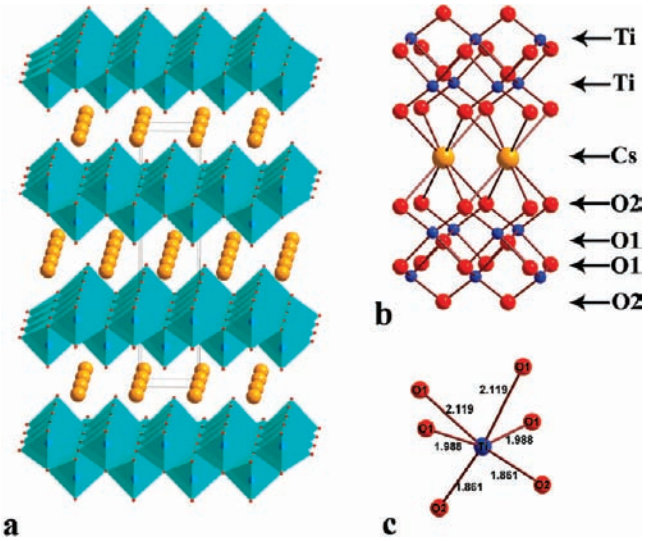

Figure 2. (a) Polyhedral representation of the crystal structure of $Cs_xTi_{2-x}Ni_{x/2}O_4$ ($x = 0.7$) viewed along the c axis of the orthorhombic unit cell. Note that Ti and Ni are indistinguishable in the structure. (b) Coordination of the atoms in the titanate. (c) Distorted TiO_6 octahedron.

corner- and edge-shared TiO_6 octahedral sheet (Figure 2b). The interlayer Cs ions are located slightly off-centered within rectangular prisms of eight two-coordinated O atoms, four from one layer and four from the next, resulting in four long Cs−O2 bonds, 3.446(2) Å, and four short Cs−O2 bonds, 3.013(2) Å. There are in addition two four-coordinated O1 atoms at a separation of 3.756(3) Å. Only 70% of the interlayer sites are occupied randomly by the Cs^+ ions, and the rest are vacant. As shown in Figure 2c, the MO_6 octahedron (M = Ti, Ni) is heavily distorted, characterized by two longer M−O1 bonds, 2.119(2) Å, and two short M−O2 bonds, 1.861(2) Å. M is therefore displaced toward the O2−O2 edges (Figure 2b). These features are more prominent than those for most other d^0 Ti^{4+} compounds and considerably different from the quite symmetric TiO_6 octahedra in anatase or rutile.[35]

The as-prepared $Cs_xTi_{2-x/2}Ni_{x/2}O_4$ is converted into the corresponding protonic form by ion exchange. The XRD data in Figure 3 show that the obtained protonic titanate retains the *I*-centered orthorhombic structure yet with a major expansion of the b axis; $a = 3.7885(4)$ Å, $b = 17.4035(3)$ Å, and $c = 2.9821(2)$ Å. Its interlayer distance is about 8.70 Å. The increased interlayer distance of 8.70 Å compared to 8.46 Å for the as-prepared $Cs_xTi_{2-x/2}Ni_{x/2}O_4$ indicates that the interlayer Cs ions have been exchanged with protons in the form of H_3O^+.[13,14,16,19,21,23]

As-prepared $Cs_xTi_{2-x/2}Ni_{x/2}O_4$ appears in the form of microcrystalline powders of micrometer dimensions and platelike morphology (Figure 4a). After acid exchange, the resulting protonic titanate maintains the platelike morphologies, although a certain degree of degradation is observed (Figure 4b). Chemical analysis (Figure 5) indicates that most of the interlayer Cs ions have been extracted, whereas the Ni substituents are preserved; compare the analyzed Ni/Ti ratio of 0.23 for as-prepared

(35) Burdett, J. K.; Hughbanks, T.; Miller, G. J.; Richardson, J. W., Jr.; Smith, J. V. *J. Am. Chem. Soc.* **1987**, *109*, 3639–3646.

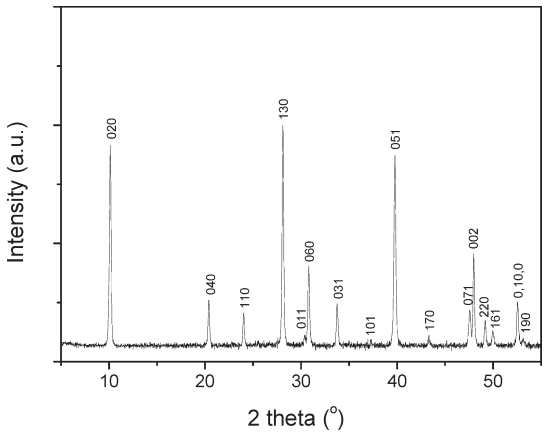

Figure 3. Powder XRD pattern of the protonic form of $Cs_xTi_{2-x/2}Ni_{x/2}O_4$ ($x = 0.7$). Wavelength: 1.540 598 Å.

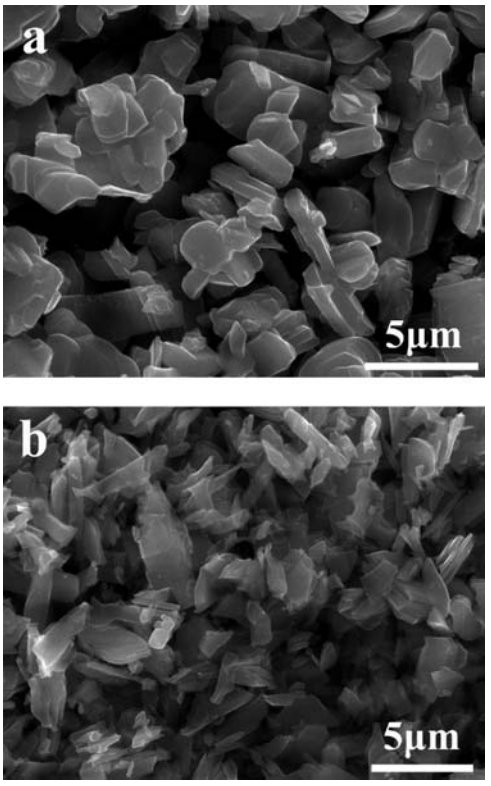

Figure 4. SEM images of (a) $Cs_xTi_{2-x/2}Ni_{x/2}O_4$ ($x = 0.7$) and (b) its protonic form.

and ion-exchanged $Cs_xTi_{2-x/2}Ni_{x/2}O_4$ (Figure 5). Ni atoms appear, hence, immobile during acid exchange,[17,23] whereas the Li, Mg, and Zn substituents of isomorphous $Cs_xTi_{2-x/3}Li_{x/3}O_4$,[14] $Cs_xTi_{2-x/2}Mg_{x/2}O_4$,[13b] and $Cs_xTi_{2-x/2}Zn_{x/2}O_4$[16] are extractable upon protonation. Apparently, the physiochemical properties of the dopants/substituents play important roles in interlayer chemistry. In this study, around 80% of the interlayer Cs ions are exchanged by protons after 3 days of acid leaching, giving $H_{0.56}Cs_{0.14}Ti_{1.65}Ni_{0.35}O_4 \cdot yH_2O$ as the composition for the resulting protonic titanate. The water content $y \approx 0.57$ is obtained according to a 5.3% weight loss from 40 to 180 °C (see Figure S2 in the Supporting Information) and supports the picture of incorporated H_3O^+ ions. Probably, the composition of the protonic titanate can be tuned

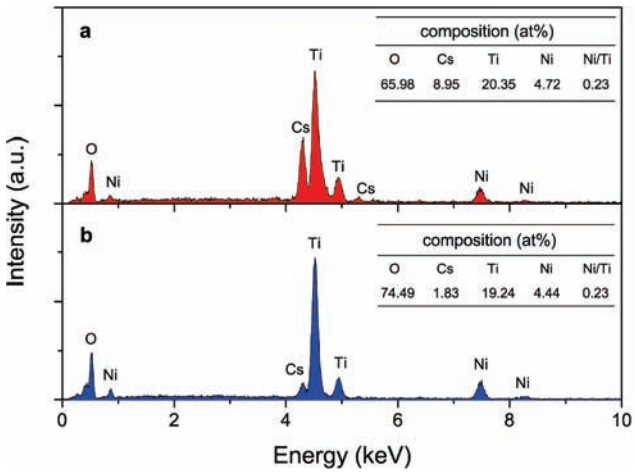

Figure 5. EDX data of (a) $Cs_xTi_{2-x/2}Ni_{x/2}O_4$ ($x = 0.7$) and (b) its protonic form. Estimated experimental error < 5%.

depending on the conditions for acid treatment; i.e., $H_yCs_{0.7-y}Ti_{2-x/2}Ni_{x/2}O_4 \cdot yH_2O$. This indicates that the residual Cs ions in the protonic titanate are probably not hydrated, which is also in agreement with the XPS analysis (see Figure S3 in the Supporting Information). We adopt the simplified formulation $H_xTi_{2-x/2}Ni_{x/2}O_4 \cdot xH_2O$ in this paper for the protonic form of $Cs_xTi_{2-x/2}Ni_{x/2}O_4$.

An attempt to delaminate the Ni-doped titanates into its molecular single sheets, $[Ti_{1-x/4}Ni_{x/4}O_2]^{-x/2}$, was made by following the well-established amine intercalation procedures.[14,16,19−21] The powder XRD pattern in Figure 6a shows, however, that the product does not have a lamellar structure with gallery heights matching the sizes of the TBA ions employed (0.95−1.05 nm in diameter),[16,20,36] but rather corresponds to that of $H_xTi_{2-x/2}Ni_{x/2}O_4 \cdot xH_2O$ in Figure 3. A very modest degree of exfoliation/delamination may have been achieved as indicated by the weak, broad reflection at $2\theta \approx 5.13°$ ($d \approx 1.72$ nm). The scanning electron microscopy (SEM) image (Figure 6b) shows basically particles with platelike morphology. Hence, the experimental data reveal that the titanate $H_xTi_{2-x/2}Ni_{x/2}O_4 \cdot xH_2O$ does not possess a delamination capability comparable to that of the isomorphous Co-doped phases[17] at the chosen conditions. This suggests that the interactions between the octahedral layers and the interlayer species might correlate to the chemical nature of lattice substituents/dopants. Therefore, changing the Ni-doping content may open the possibility of modifying the interlayer chemistry. We will discuss this possibility later in this paper.

XPS. Figure 7 reports the XPS survey spectra of $Cs_xTi_{2-x/2}Ni_{x/2}O_4$ and $H_xTi_{2-x/2}Ni_{x/2}O_4 \cdot xH_2O$. Photoelectron peaks of Cs, Ti, Ni, O, and C and Auger peaks of Ni *LMM*, Ti *LMM*, Cs *MNN*, and O *KLL* are observed. The C signal at 284.8 eV represents most likely surface contaminations.[30] The loss of Cs ions during acid exchange is evident from the intensity of the Cs photoelectron peaks in Figure 7b; moreover, the same binding energies of the Cs photoelectrons (see Figure S3 in the Supporting Information) reveal that the residual Cs ions

(36) Gao, Q.; Giraldo, O.; Tong, W.; Suib, S. L. *Chem. Mater.* **2001**, *13*, 778–786.

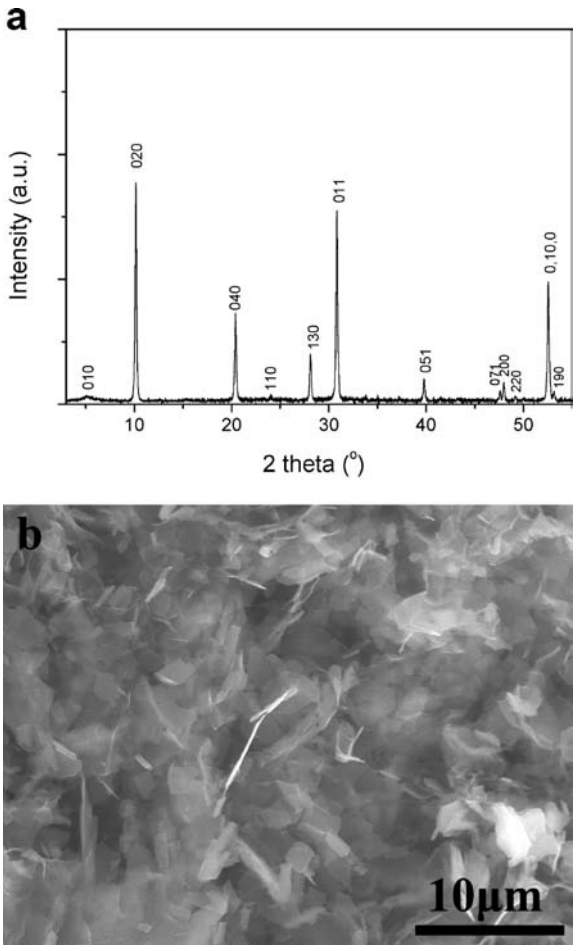

Figure 6. Powder XRD pattern with Miller indices (a) and the SEM image (b) of $H_xTi_{2-x/2}Ni_{x/2}O_4 \cdot xH_2O$ exposed to TBA. Wavelength: 1.540 598 Å.

in $H_xTi_{2-x/2}Ni_{x/2}O_4 \cdot xH_2O$ have the same anionic coordinations as those in the $Cs_xTi_{2-x/2}Ni_{x/2}O_4$.

Figure 8 reports Ni 2p XPS spectra. In addition to the Ni $2p_{3/2}$ and Ni $2p_{1/2}$ main peaks, well-known shakeup satellites are clearly seen;[37−39] see Table 4 for the peak positions and peak splittings. The binding energy of the predominant Ni $2p_{3/2}$ peak is 854.6 eV, being separated by 6.0 eV from its shakeup satellite. The reported binding energies for the Ni $2p_{3/2}$ peaks in NiO, $Ni(OH)_2$, and $NiSO_4$ are 854, 856, and 857 eV, respectively,[39,40] exhibiting thus a significant variation even though Ni is divalent. It reveals clearly the role of the ionicity of materials in their charging effects. Nesbitt et al. suggested that the binding-energy shifts of Ni-containing insulators do not result from variations in the oxidation state of Ni but rather reflect changes in the nature of the connected anions.[39] This seems in line with the variation currently observed for the Ni 2p peaks at different stages of the acid-exchange process (Figure 8 and Table 4). It is

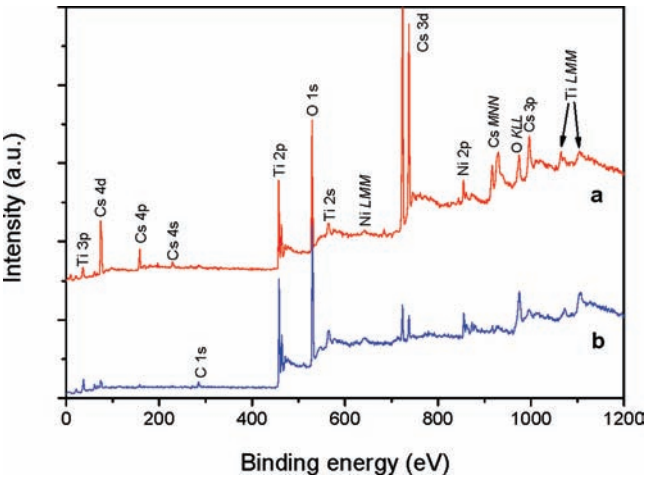

Figure 7. XPS survey spectra of (a) $Cs_xTi_{2-x/2}Ni_{x/2}O_4$ and (b) $H_xTi_{2-x/2}Ni_{x/2}O_4 \cdot xH_2O$.

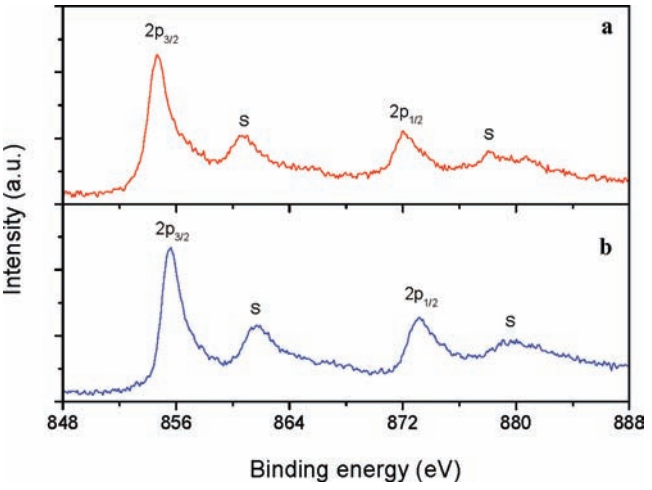

Figure 8. Ni 2p XPS spectra of (a) $Cs_xTi_{2-x/2}Ni_{x/2}O_4$ and (b) $H_xTi_{2-x/2}Ni_{x/2}O_4 \cdot xH_2O$. S indicates the shakeup satellite.

Table 4. Ni 2p Binding Energy and Peak Splitting for $Cs_xTi_{2-x/2}Ni_{x/2}O_4$ and $H_xTi_{2-x/2}Ni_{x/2}O_4 \cdot xH_2O$

compound	$2p_{3/2}$ (eV)[a]	ΔSat (eV)[b]	$2p_{1/2}$ (eV)[a]	Δ2p (eV)[c]
$Cs_xTi_{2-x/2}Ni_{x/2}O_4$	854.6	6.0	872.0	17.4
$H_xTi_{2-x/2}Ni_{x/2}O_4 \cdot xH_2O$	855.6	6.0	873.1	17.5

[a] Estimated experimental error ±0.2 eV. [b] Separation between the main $2p_{3/2}$ peak and its associated shakeup satellite. [c] Separation between the $2p_{3/2}$ and $2p_{1/2}$ photoelectron peaks.

observed that the binding energies of Ni 2p in $H_xTi_{2-x/2}Ni_{x/2}O_4 \cdot xH_2O$ are about 1 eV higher than those for $Cs_xTi_{2-x/2}Ni_{x/2}O_4$ (Table 4). As shown in Figure 2c, the Ni atoms are bonded to six O atoms, of which four are four-coordinated O1 and two are two-coordinated O2. The latter O atom bonds, furthermore, to the interlayer Cs ions (Figure 2b). The exchange of Cs ions with protons results in changes in the binding nature of the Ni−O2−Cs/H bonds. This is probably rather analogous to the shift in the binding energy of the Ni $2p_{3/2}$ peak

(37) Cristina Oliveira, M.; Botelho do Rego, A. M. *J. Alloys Compd.* **2006**, *425*, 64–68.
(38) (a) Wertheim, G. K.; Hüfner, S. *Phys. Rev. Lett.* **1972**, *28*, 1028–1031. (b) Hüfner, S.; Wertheim, G. K. *Phys. Rev. B* **1973**, *8*, 4857–4867.
(39) Nesbitt, H. W.; Legrand, D.; Bancroft, G. M. *Phys. Chem. Minerals* **2000**, *27*, 357–366.
(40) (a) Legrand, D. L.; Nesbitt, H. W.; Bancroft, G. M. *Am. Mineral.* **1998**, *83*, 1256–1265. (b) Matienzo, L. J.; Yin, L. I.; Grim, S. O.; Schwartz, W. E. *Inorg. Chem.* **1973**, *12*, 2762–2769.

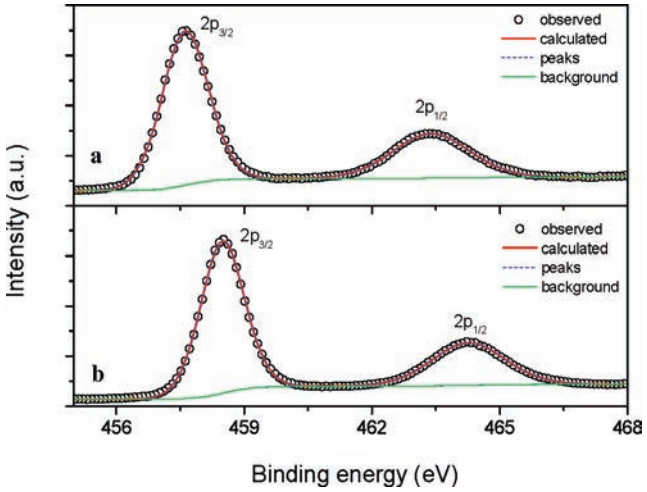

Figure 9. Ti 2p XPS spectra of (a) $Cs_xTi_{2-x/2}Ni_{x/2}O_4$ and (b) $H_xTi_{2-x/2}Ni_{x/2}O_4 \cdot xH_2O$.

Table 5. Ti 2p Binding Energy and Energy Splitting for $Cs_xTi_{2-x/2}Ni_{x/2}O_4$ and $H_xTi_{2-x/2}Ni_{x/2}O_4 \cdot xH_2O$

compound	$2p_{3/2}$ (eV)[a]	$2p_{1/2}$ (eV)	Δ_{2p} (eV)[b]	$2p_{3/2}$: $2p_{1/2}$ intensity ratio[c]
$Cs_xTi_{2-x/2}Ni_{x/2}O_4$	457.6 (1.2)[d]	463.3 (2.1)	5.7	2.1:1.00
$H_xTi_{2-x/2}Ni_{x/2}O_4 \cdot xH_2O$	458.5 (1.2)	464.2 (2.0)	5.7	2.1:1.00

[a] Estimated experimental error ±0.2 eV. [b] Separation between the $2p_{3/2}$ and $2p_{1/2}$ photoelectron peaks. [c] Integrated intensity according to the contribution of each peak to the total number of counts under the $2p_{3/2}$ and $2p_{1/2}$ peaks. [d] Values in brackets are the full width at half-maximum of the peaks.

between NiO (853.7 eV) and $Ni(OH)_2$ (856.2 eV).[39,40] A similar phenomenon and explanation may naturally also apply for Ti photoelectron peaks (Figure 9).

The Ti 2p XPS spectra in Figure 9 of $Cs_xTi_{2-x/2}Ni_{x/2}O_4$ and $H_xTi_{2-x/2}Ni_{x/2}O_4 \cdot xH_2O$ exhibit symmetrical profiles, revealing a single oxidation state for the Ti atoms.[16] In the protonic form, the Ti 2p peaks are shifted to higher binding energies (Table 5) similar to those observed for the Ni 2p peaks (see above). Because a violent redox reaction such as $Ti^{4+} \rightarrow Ti^{5+}$ cannot be expected in an acid-exchange reaction,[16,41] we suggest that the same mechanism is operative, as described for the Ni 2p peaks. This is in harmony with changes in the binding nature on going from Ti−O2−Cs to Ti−O2−H. A more detailed analysis on the binding-energy shift of the Ti 2p peaks has been reported for a Zn-doped titanate $Cs_xTi_{2-x/2}Zn_{x/2}O_4$ ($x = 0.7$).[16]

As shown in Figure 2b, the structure contains two nonequivalent O atoms: four-coordinated O1 and two-coordinated O2. The former bonds solely to intralayer cations such as Ti and Ni, whereas the second bonds also to the interlayer species such as Cs ions. Therefore, different O 1s binding energies can be expected.[16,42] The chemical environments of the two-coordinated O2 will change dramatically when Cs is exchanged with protons,

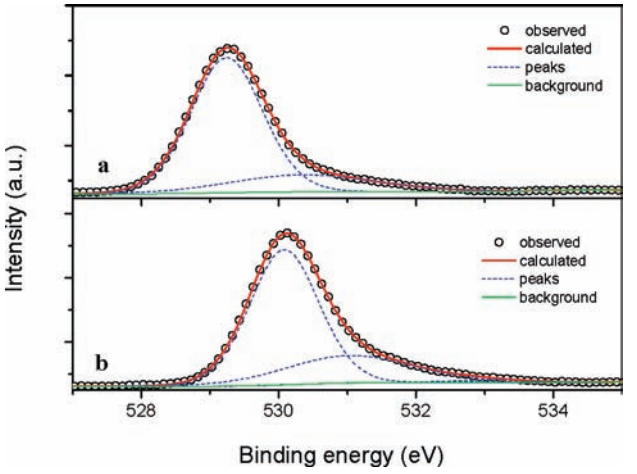

Figure 10. O 1s XPS spectra of (a) $Cs_xTi_{2-x/2}Ni_{x/2}O_4$ and (b) $H_xTi_{2-x/2}Ni_{x/2}O_4 \cdot xH_2O$.

Table 6. O 1s Binding Energy for $Cs_xTi_{2-x/2}Ni_{x/2}O_4$ and $H_xTi_{2-x/2}Ni_{x/2}O_4 \cdot xH_2O$

compound	O2 (eV)[a]	O1 (eV)	H_2O (eV)
$Cs_xTi_{2-x/2}Ni_{x/2}O_4$	529.1 (1.2)[b]	530.5 (2.5)	
$H_xTi_{2-x/2}Ni_{x/2}O_4 \cdot xH_2O$	530.0 (1.2)	530.8 (2.1)	532.9 (1.4)

[a] Estimated experimental error ±0.2 eV. Oxygen with different coordination numbers (e.g., Table 2). [b] Values in brackets are the full width at half-maximum of the peaks.

whereas that for the four-coordinated O1 remains unchanged. A possible complicating factor is the additional signal from water O atoms for the protonated compound. However, this signal occurs at much higher binding energies; see Table 6. As reported in Figure 10 and Table 6, the higher binding energy for the O2 species in $H_xTi_{2-x/2}Ni_{x/2}O_4 \cdot xH_2O$ can be understood in line with changes in the bond characteristics between O2−Cs (in $Cs_xTi_{2-x/2}Ni_{x/2}O_4$) and O2−H ($H_xTi_{2-x/2}Ni_{x/2}O_4 \cdot xH_2O$).

Raman Scattering Spectroscopy. As displayed in Figure 11, the Raman scattering spectrum of $Cs_xTi_{2-x/2}Ni_{x/2}O_4$ has the same basic features as that of the protonic titanate $H_xTi_{2-x/2}Ni_{x/2}O_4 \cdot xH_2O$ because of their similar crystal structures. However, differences are also noticeable, especially in the high wavenumber region, 700−950 cm^{-1}.

A definitive assignment of the observed Raman bands in Figure 11 is not possible without lattice dynamical calculations and/or polarized Raman scattering spectra on single-crystal samples. Nevertheless, some preliminary considerations can be done. For example, the spectrum in Figure 11b shows much similarity to that for $H_xTi_{2-x/4}\square_{x/4}O_4 \cdot H_2O$ ($x = 0.7$, $\square$ = vacancy), having nine Raman modes at 183, 270, 387, 449, 558, 658, 704, 803, and 908 cm^{-1}.[21] Both of these phases consist of similar 2D lepidocrocite-type octahedral host layers. Usually, the Raman bands at 700−950 cm^{-1} are correlated to stretching vibrations of the short Ti−O2 bonds that stick out into the interlayer space,[21,29] with their intensities and positions reflecting the nature of the substituents and the interlayer species.[13b] Hence, the peaks at 851 and 910 cm^{-1} for $H_xTi_{2-x/2}Ni_{x/2}O_4 \cdot xH_2O$ (Figure 11b) have probably the same origins as the 803 and 908 cm^{-1} bands for $H_xTi_{2-x/4}\square_{x/4}O_4 \cdot H_2O$.[21] The energy shifts can be attributed

(41) (a) Perkins, C. L.; Henderson, M. A.; McCready, D. E.; Herman, G. S. *J. Phys. Chem. B* **2001**, *105*, 595–596. (b) Weast, R. C. *CRC Handbook of Chemistry and Physics*, 64th ed.; CRC Press: Boca Raton, FL, 1984.
(42) McIntyre, N. S.; Zetaruk, D. G. *Anal. Chem.* **1977**, *49*, 1521–1529.

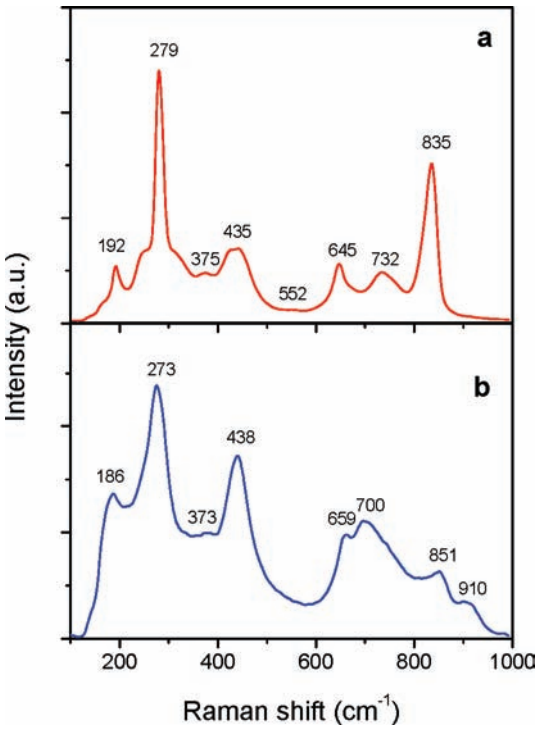

Figure 11. Raman scattering spectrum of (a) $Cs_xTi_{2-x/2}Ni_{x/2}O_4$ and (b) $H_xTi_{2-x/2}Ni_{x/2}O_4 \cdot xH_2O$.

to the local structural features induced by Ni atoms or Ti vacancies.[13b] During acid exchange, the sharp, intense Raman band at 835 cm^{-1} of $Cs_xTi_{2-x/2}Ni_{x/2}O_4$ (Figure 11a) shifts to 851 cm^{-1} for $H_xTi_{2-x/2}Ni_{x/2}O_4 \cdot xH_2O$, indicating that the interlayer species strongly affect the stretching vibrations of the short Ti−O2 bonds. Similar phenomena are reported previously for isomorphous layered $Cs_2Ti_2O_5$ and $K_2Ti_2O_5$,[29] where changes were observed also in the high-wavenumber region, 850−950 cm^{-1}, because of the different vibrational features between Ti−O−Cs and Ti−O−K.

Magnetic Properties. The incorporation of Ni cations into octahedral sites of the titanate will influence its magnetic behavior. Because of possible trace amounts of, e.g., NiO, in the starting cesium titanates (e.g., as indicated by the asterisk in Figure 1), the protonic forms were presently analyzed. As shown in Figure 12a, the magnetic susceptibility for $H_xTi_{2-x/2}Ni_{x/2}O_4 \cdot xH_2O$ exhibits typical paramagnetic behavior in the temperature range 5−350 K. The inverse magnetic susceptibility can be well described according to the Curie−Weiss relation[43]

$$\chi = C/(T-\theta) \qquad (1)$$

where C is the Curie constant, T is the absolute temperature, and θ is the Weiss temperature. The calculated Weiss temperature is about −2.51(1) K. An effective magnetic moment of $\mu_{eff} = 1.57(1)\,\mu_B$ is obtained, in agreement with the theoretical value 1.67 μ_B within experimental error.[44] Figure 12b displays the dependence of magnetization on the magnetic field at a temperature of 5 K. The measured

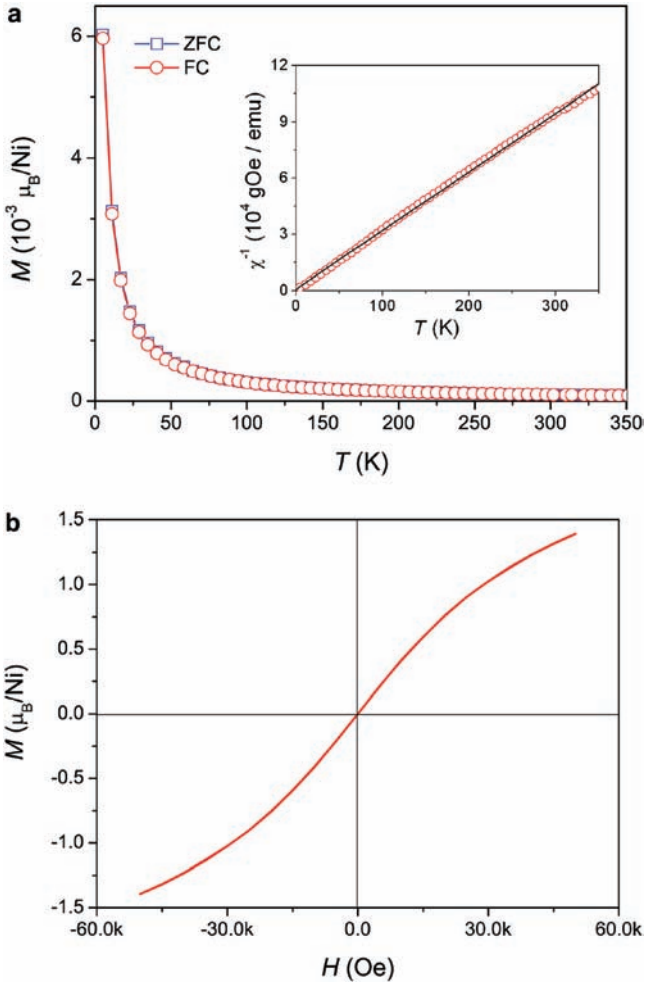

Figure 12. (a) ZFC and FC magnetization curves of $H_xTi_{2-x/2}Ni_{x/2}O_4 \cdot xH_2O$. Applied field: 100 Oe. The inset shows the temperature dependence of the inverse magnetic susceptibility; a representative fit of the Curie−Weiss law is shown as a straight line. (b) $M-H$ curve of $H_xTi_{2-x/2}Ni_{x/2}O_4 \cdot xH_2O$ at 5 K.

$M-H$ curve does not show any obvious hysteresis loops,[43] showing typical paramagnetic behavior for the $H_xTi_{2-x/2}Ni_{x/2}O_4 \cdot xH_2O$.

Similar paramagnetic behaviors have widely been reported for Ni-doped TiO_2[45−48] and titanates.[8,49] For example, Park et al. predicted a paramagnetic ground state for Ni-doped TiO_2 by using local-spin-density calculations.[46] On the basis of ab initio calculation, Errico et al. suggested that a local magnetic moment could appear in Mn-, Fe-, and Co-doped TiO_2 but interestingly not in Ni-doped TiO_2.[47] Hong et al. claimed room-temperature ferromagnetism in Ni-doped TiO_2 films grown by laser ablation;[24] however, the possible formation of nickel or nickel oxide clusters must be carefully considered.[25,48]

(43) O'Handley, R. C. *Modern magnetic materials: principles and applications*; Wiley: New York, 2000.
(44) Calculated spin-only moment according to $\mu_{eff}^2 = 1.65\mu_{eff}(Ti^{4+})^2 + 0.35\mu_{eff}(Ni^{2+})^2$.

(45) Uhm, Y. R.; Woo, S. H.; Kim, W. W.; Kim, S. J.; Rhee, C. K. *J. Magn. Magn. Mater.* **2006**, *304*, e781–e783.
(46) Park, M. S.; Kwon, S. K.; Min, B. I. *Phys. Rev. B* **2002**, *65*, 161201 (4 pages).
(47) Errico, L. A.; Renteria, M.; Weissmann, M. *Phys. Rev. B* **2005**, *72*, 184425 (8 pages).
(48) Glaspell, G.; Panda, A. B.; EI-Shall, M. S. *J. Appl. Phys.* **2006**, *100*, 124307 (6 pages).
(49) Wang, M. L.; Song, G. B.; Li, J.; Miao, L. D.; Zhang, B. S. *J. Univ. Sci. Technol. Beijing* **2008**, *15*, 644–648.

Wang et al. observed that titanate nanotubes doped with Ni atoms displayed typical paramagnetic behaviors.[49]

Some theoretical approaches suggest also ferromagnetism in Ni-doped TiO_2;[50,51] however, the presence of oxygen vacancies appears to be critical. For example, Chen et al. claimed that a ferromagnetic insulating ground state appears when two Ni atoms are associated with one oxygen vacancy, with the magnetic origin being Ni^{3+} ions.[50] Neither oxygen vacancies nor Ni^{3+} ions are likely for the current Ni-doped lepidocrocite titanates. These titanates rather prefer cationic vacancies, as evidenced by $Cs_xTi_{2-x/4}\square_{x/4}O_4$[10,11] and $H_xTi_{2-x/4}\square_{x/4}O_4\cdot H_2O$ ($x = 0.7$, $\square$ = vacancy).[14,19−21] Therefore, the vacancy-mediated mechanism[50] is not applicable. We also note that preliminary results on Ni−Mg-codoped titanates with varied Ni-doping contents show typical paramagnetic behavior with magnetic moments being tuned by Ni-doping levels (see Figure S4 in the Supporting Information). We therefore conclude that pure Ni-substituted lepidocrocite titanates do not exhibit ferromagnetism.

Ni−Mg-Codoped Titanates $Cs_xTi_{2-x}(Ni_yMg_{1-y})_{x/2}O_4$ ($x = 0.7$, $0 \le y \le 1$). Because of the strict charge-compensation mechanism in $Cs_xTi_{2-x/2}Ni_{x/2}O_4$, it is difficult to vary the Ni content over significant ranges. However, it is feasible to vary the Ni concentration at the Ti site by introducing Ni and Mg cosubstitution, i.e., $Cs_xTi_{2-x/2}(Ni_yMg_{1-y})_{x/2}O_4$ ($0 \le y \le 1$). The divalent Ni^{2+} and Mg^{2+} ions will maintain the described charge compensation scheme and thus prevent any phase separation. This may allow elucidation of likely doping-dependent physiochemical properties. Actually, a more general formulation can be given as $Cs_xTi_{2-x/2}(M_yN_{1-y})_{x/2}O_4$ ($x = 0.7$ and $0 \le y \le 1$), with M and N being any two of the divalent metals such as Ni, Zn, Mg, Cu, and Co. It may open also the possibility of achieving multifunctionality in lepidocrocite titanates by rationally selecting the lattice dopants. It shall be emphasized that this substitution scheme is clearly different from that reported previously for $K_{0.8}Ti_{1.6-x/2}Fe_xCo_{0.4-x/2}O_4$ ($x = 0-0.8$),[17c] where the incorporation of Fe^{3+} and Co^{2+} ions in the host layer will also influence the Ti content (or the interlayer cation concentration), which readily triggers phase separation during synthesis.

Samples were prepared for the solid solution $Cs_xTi_{2-x}(Ni_yMg_{1-y})_{x/2}O_4$ ($x = 0.7$ and $0 \le y \le 1$) with Ni contents $y = 0$, 0.14, 0.28, 0.56, 0.85, and 1. XRD patterns of the obtained isostructural, lepidocrocite-type samples are displayed in Figure 13. It shall be emphasized that the as-prepared titanate $Cs_xTi_{2-x}(Ni_yMg_{1-y})_{x/2}O_4$ retains the lepidocrocite-type layered structure over the doping concentration range covered, revealing clearly that an intrinsic codoping of Ni and Mg has successfully been achieved. The random distribution of Mg and Ni within the layers was confirmed by Rietveld refinements based on SXRD data of an intermediate composition $Cs_{0.7}Ti_{1.65}Ni_{0.20}Mg_{0.15}O_4$ (see Figure S5 and Table S1 in the Supporting Information).

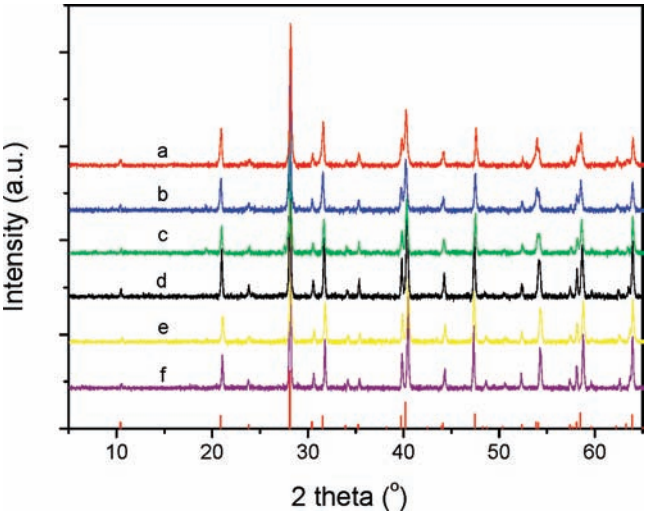

Figure 13. Powder XRD patterns, shifted vertically for comparison, for $Cs_xTi_{2-x}(Ni_yMg_{1-y})_{x/2}O_4$ ($x = 0.7$ and $0 \le y \le 1$). $y = 0$, 0.14, 0.28, 0.56, 0.85, and 1 for patterns a−f, respectively. Positions and tabulated intensities are indicated by the vertical bars, bottom. Wavelength: 1.540 598 Å.

Table 7. Unit Cell Dimensions for $Cs_xTi_{2-x}(Ni_yMg_{1-y})_{x/2}O_4$ ($x = 0.7$ and $0 \le y \le 1$)[a]

compound	a (Å)	b (Å)	c (Å)	V(Å^3)
$Cs_{0.7}Ti_{1.65}Ni_{0.00}Mg_{0.35}O_4$[b,c]	3.8283(1)	17.0060(6)	2.9799(2)	194.00(1)
$Cs_{0.7}Ti_{1.65}Ni_{0.05}Mg_{0.30}O_4$	3.8293(1)	17.0047(8)	2.9800(2)	194.04(1)
$Cs_{0.7}Ti_{1.65}Ni_{0.10}Mg_{0.25}O_4$	3.8313(1)	16.9887(7)	2.9776(0)	193.81(1)
$Cs_{0.7}Ti_{1.65}Ni_{0.20}Mg_{0.15}O_4$	3.8370(1)	16.9495(6)	2.9742(2)	193.43(1)
$Cs_{0.7}Ti_{1.65}Ni_{0.30}Mg_{0.05}O_4$	3.8425(1)	16.9244(5)	2.9704(1)	193.17(1)
$Cs_{0.7}Ti_{1.65}Ni_{0.35}Mg_{0.00}O_4$	3.8430(1)	16.9192(4)	2.9682(1)	192.99(1)

[a] Calculated standard deviations are in parentheses. [b] Reference 13a: $a = 3.827(2)$ Å, $b = 17.03(1)$ Å, and $c = 2.981(3)$ Å. [c] Reference 13b: $a = 3.828325(23)$ Å, $b = 17.00643(11)$ Å, and $c = 2.981444(20)$ Å.

As reported in Table 7, the unit cell dimensions for the $Cs_xTi_{2-x}(Ni_yMg_{1-y})_{x/2}O_4$ solid solution vary nearly linearly with the Ni level. The b and c axes, as well as the unit cell volume V, decrease with increasing Ni content, whereas the a axis increases. The fact that the interlayer distance decreases with increasing Ni doping may reflect changes in the electrostatic interactions between the 2D octahedral host layers and interlayer species, possibly correlated with the electronegativity of the involved elements, 1.91 for Ni and 1.31 for Mg.[52] The difference in the ionic size, Ni^{2+} ions of 0.70 Å and Mg^{2+} ions of 0.72 Å,[53] is probably not a key factor. This observation may possibly be relevant also for explaining the poor delamination capability of $H_xTi_{2-x/2}Ni_{x/2}O_4\cdot xH_2O$ in comparison with that of the $H_xTi_{2-x/2}O_{4-x/2}\cdot H_2O$, i.e., the protonic form of $Cs_xTi_{2-x/2}Mg_{x/2}O_4$.[13b]

Figure 14 shows that the interlayer chemistry of the studied titanates depends strongly on the Ni content. The end member $Cs_xTi_{2-x/2}Mg_{x/2}O_4$ has excellent amine-intercalation capabilities, as evidenced by well-defined ($0k0$) XRD reflections.[13b] Moreover, the incorporation of TBA ions into the interlayer spaces will at the same

(50) Chen, J.; Lu, G. H.; Cao, H. H.; Wang, T. M.; Xu, Y. *Appl. Phys. Lett*. **2008**, *93*, 172504 (3 pages).
(51) Peng, H. W.; Li, J. B.; Li, S. S.; Xia, J. B. *J. Phys.: Condens. Matter* **2008**, *20*, 125207 (6 pages).
(52) Huheey, J. E. *Inorganic Chemistry: Principles of structure and reactivity*, 3rd ed.; Harper & Row: New York, 1983.
(53) Shannon, R. D.; Prewitt, C. T. *Acta Crystallogr*. **1969**, *B25*, 925–946.

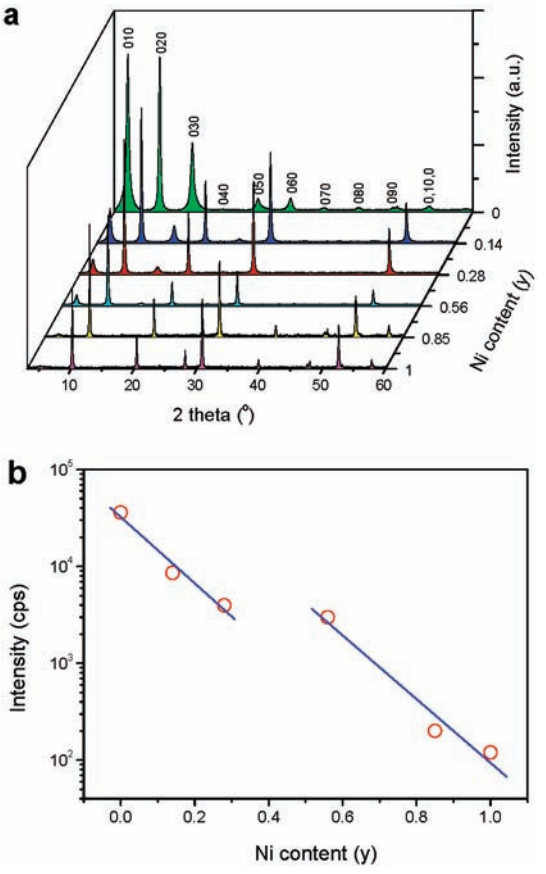

Figure 14. (a) XRD patterns for amine-intercalated $Cs_xTi_{2-x}(Ni_yMg_{1-y})_{x/2}O_4$ ($x = 0.7$ and $0 \leq y \leq 1$) showing strongly decreasing product formation upon increasing Ni content. (b) Variation in the intensity of (010) for the amine-intercalated titanates. Estimated error < 5%; solid lines are drawn only to guide the eye.

time trigger delamination of $Cs_xTi_{2-x/2}Mg_{x/2}O_4$ (actually of its protonic form) into molecular 2D sheets and a thickness of ca. 1 nm.[13b] This capability is also observed for $Cs_xTi_{2-x}(Ni_yMg_{1-y})_{x/2}O_4$ with low Ni contents, $0 \leq y \leq 0.28$. In contrast, the Ni-enriched samples, i.e., $0.56 \leq y \leq 1$, can barely be delaminated. Moreover, although the intensity of (010) for the TBA-intercalated compounds is seen to decrease with increasing Ni content, the physicochemical behavior of the Ni-enriched samples is apparently different from that of low Ni contents (Figure 14b). This can be accounted for by the different chemical nature such as the electronegativity of the Mg and Ni atoms.[16,52] It is worth pointing out that the Mg atoms in $Cs_xTi_{2-x/2}Mg_{x/2}O_4$ are exchangeable,[13b] whereas the Ni atoms of $Cs_xTi_{2-x/2}Ni_{x/2}O_4$ are immobile upon protonation (e.g., Figure 5). However, both of the Ni and Mg atoms appear to be immobile during acid exchange of the titanate $Cs_xTi_{2-x}(Ni_yMg_{1-y})_{x/2}O_4$, of which the details are still unclear. This may imply that the different lattice dopants in the titanate lattice would affect each other, suggesting interesting applications for the studies on the dopant-dependent physiochemical properties of lepidocrocite titanates. Further studies along this line are underway.

Conclusions

Ni-doped lepidocrocite titanate $Cs_xTi_{2-x/2}Ni_{x/2}O_4$ and its protonic derivative $H_xTi_{2-x/2}Ni_{x/2}O_4 \cdot xH_2O$ ($x = 0.7$) are prepared and characterized. SXRD data show that the Ni atoms substitute for Ti and are randomly distributed in the octahedral host layers, thereby producing negatively charged layers that are compensated for by interlayer Cs ions. Raman scattering data show that the exchange of interlayer Cs ions with protons H_3O^+ results in significant changes in the local structure. The observed shifts in XPS binding energies for Ni and Ti photoelectrons correlate with the bonding features of O atoms in the first coordination sphere. The Ni substitution introduces paramagnetic properties; the effective paramagnetic moment $\mu_{eff} = 1.57(1)\ \mu_B$ and the Curie−Weiss temperature −2.51(1) K are obtained for $H_xTi_{2-x/2}Ni_{x/2}O_4 \cdot xH_2O$. Several features of the crystal structure, interlayer chemistry, and magnetic properties are doping-dependent and can be modified and tuned. The methodology developed can be employed for studies on the interlayer chemistry and defect chemistry of other layered compounds.

Acknowledgment. The authors acknowledge financial assistance from the Research Council of Norway through the NANOMAT program (163565/431 and 158518/431) and the NanoEnvironment project. SXRD beam time is made available at SNBL, ESRF, through Proposal 01-01-760.

Supporting Information Available: XRD, TGA, and magnetic measurements on some Ni-doped titanates. This material is available free of charge via the Internet at http://pubs.acs.org.